Studies of Organometallic Self-Assembled Monolayers on Ag and Au Using Surface Plasmon Spectroscopy

Timothy T. Ehler, Nathan Malmberg, Keith Carron, B. Patrick Sullivan, and Lewis J. Noe*

Department of Chemistry, University of Wyoming, Laramie, Wyoming 82071

Received: November 18, 1996; In Final Form: February 5, 1997[⊗]

We report the synthesis of a novel rhenium complex, {*fac*-Re(2,2′-bipyridine)$(CO)_3(NC_5H_4)CH_2NHCO(CH_2)_2S-\}_2$ and its self-assembly behavior on Ag and Au, including characterization of the monolayer using surface plasmon spectroscopy (SPS). Further surface characterization, which proved to be quite complementary to SPS, was accomplished with surface-enhanced Raman spectroscopy (SERS), FTIR, ellipsometry, and contact angle measurements. SERS and FTIR data have also been used to verify the self-assembly of the free ligand and rhenium complexes on Ag to form monolayers (SAMs). Vibrational analysis also provided evidence that the attachment of the free ligand and complexes to the metal substrate occurs by reaction of the disulfide bond and not through the pyridine or bipyridine. The tilt angle of the complex with respect to the surface normal of the metal was also calculated using a projection analysis that incorporated the SPS determined thickness and a molecular mechanics (MM) minimized molecular length. Independently, a MM tilt angle was determined by minimization of a hexagonal grouping of six complexes surrounding one, each bound through a sp hybridized S-metal bond to a hollow surface site. Though this calculation is in need of further refinement, the agreement with our projection analysis is good.

Introduction

There is currently a great deal of interest in materials research on thin organic, organometallic, and polymer films exhibiting nonlinear optical properties. These interests range from the development of polymers with improved nonlinear optical performance[1] to using single molecules in sequentially building multilayer systems to producing thin-film optical devices having specific properties.[2] Until recent methods for the preparation of self-assembled monolayers (SAMs) using thin derivatized metal surfaces, the most common method of monolayer and multilayer attachment on surfaces has been accomplished by the Langmuir−Blogett (LB) approach[3] including poled polymer films doped with polar molecules.[2,4] One of the first approaches for constructing multilayers for second-order nonlinear optics was accomplished by Girling *et al*. using the LB approach involving films consisting of alternating layers of merocyanine dye and ω-tricosenoic acid.[5] Recently, SAMs have been used successfully to form multilayers of ultrathin films on a gold surface.[6−9]

A considerable amount of research has taken place in the synthesis and characterization of nonlinear organic molecules, but relatively few nonlinear organometallic materials have been explored. Because many organometallics are known to possess conjugated π-electron systems or low-lying charge-transfer states, they are capable of possessing large nonlinear polarizabilities. Metal−pyridine and bipyridine complexes have already been found to generate nonlinear signals. It has been demonstrated that solid samples of the complexes of the formulation *fac*-Re(2,2′-bipyridine)$(CO)_3X$[10,11] (X = Cl or SO_3CF_3) exhibited significant hyperpolarizability (β) values.[12] The chromophoric origin of second harmonic generation (SHG) in these molecules is through low-lying metal-to-ligand charge-transfer (MLCT) states where, upon excitation, electrons are removed from metal-based d π (Re) orbitals and placed in the lowest-lying ligand-based π *(bpy) orbital. For a series of *fac*-Re(bpy)$(CO)_3X$ complexes, interpretation of solvent dependence for the MLCT manifold is consistent with the large dipole moment change necessary for measurable nonlinear optical effects.[13] By use of this monomer as a chromophoric base, mono- and multilayer systems can be constructed.

As a prelude to future studies of nonlinear behavior, we report the synthesis of a novel rhenium complex, {*fac*-Re(2,2′-bipyridine)$(CO)_3(NC_5H_4)CH_2NHCO(CH_2)_2S-\}_2$ and its self-assembly behavior on Ag and Au, including characterization of the monolayer using surface plasmon spectroscopy (SPS). This physical method not only permits the index of refraction of the film and its thickness to be easily and accurately determined, but it also provides complementary information on the bulk molecular orientation, knowing the length of a molecular unit bonded to the metal surface via a simple projection calculation. Further surface characterization, which proved to be quite complementary to SPS, was accomplished with surface-enhanced Raman spectroscopy (SERS), ellipsometry, and contact angle measurements.

Experimental Section

Materials. 2,2′-Bipyridyl (98+%), 3,3′-dithioipropionic acid (99%), 4-(aminomethyl)pyridine (98%), 1,1′-carbonyldiimidazole (98%), Ag (99.9999%), Au (99.999%), and silver foil (99.9%, 0.1 mm) were obtained from Aldrich and used without further purification. Methylene chloride, petroleum ether, diethyl ether (anhydrous), and methanol were all Chempure grade from Curtin Matheson Scientific and were used as received. Toluene (Baker Analyzed Reagent, HPLC grade), chloroform (photorex reagent grade), acetone (ACS reagent grade), acetonitrile (photorex reagent grade) from J. T. Baker Chemicals (Phillipsburg, NJ) were used without further purification. Tetrahydrofuran from J. T. Baker Chemicals was dried using sodium/benzophenone under an Ar atmosphere, which was left to reflux for at least 1 h followed by distillation prior to use. Anhydrous ethanol (200 proof) was obtained from McCormick Distilling Co. (Weston, MO). Water was deionized using a Millipore Milli-Q system.

[⊗] Abstract published in *Advance ACS Abstracts,* April 1, 1997.

S1089-5647(96)03846-1 CCC: $14.00

Trifluoromethanesulfonic acid (CF_3SO_3H, i.e., triflic acid) was used as received from Aldrich. Trifluoromethanesulfonic anhydride [$(CF_3SO_2)_2O$, i.e., triflic anhydride] obtained from Alfa-Ventron (Danvers, MA) also was used without further purification. Pentacarbonylrhenium(I) chloride was purchased from the Pressure Chemical Co. (Pittsburgh, PA). Fisherbrand BK-7 microscope slides were rigorously cleaned and prepared as described previously[14] before being used as the substrate for the vapor-deposited metals in the surface plasmon studies.

Metal Film Preparation. *Surface Plasmon Spectroscopy and Ellipsometry*. A sample of 500 Å of Ag or Au was thermally evaporated onto clean BK-7 glass substrates using an Edwards E306A coating system as described previously.[14] Within the chamber the 25 mm × 25 mm × 1 mm BK-7 slides were placed on a specially prepared mask. The chamber was then evacuated to a pressure of $(4-6) \times 10^{-7}$ mbar, at which time the metal was vapor deposited at a rate of 1−2 Å/s. The best metal plasmon curve, one having the deepest resonance minimum was obtained by using 99.9999% Ag and 99.999% Au. A film thickness monitor (FLM), located within the coating chamber, monitored the rate and thickness of the metal film being deposited. Upon removal from the chamber, the metal-coated slides were subjected to no longer than 20 min in the atmosphere before being immersed in a solution containing the adsorbate. Control experiments indicated that there were no differences between the Ag or Au metal-coated slides immersed immediately upon removal from the vapor deposition chamber and those subjected to 20 min in the laboratory atmosphere. This length of time was necessary to collect ellipsometric or plasmon data in determining the optical constants of the pure metal films.

SERS of Ag Foil. The roughened silver substrate was prepared by cutting a 1 mm^2 piece of foil from the bulk sheet and etching in 30% nitric acid for 1 min with vigorous stirring. This substrate was then washed with Millipore water, ethanol, and air dried.

Preparation of Ligands and Complexes. *{(NC$_5$H$_4$)CH$_2$NHCO(CH$_2$)$_2$S−}$_2$*. A 2.96 g sample of 1,1′-carbonyldiimidazole (1.83 mmol) was dissolved by stirring in 50 mL of dry THF in a 100 mL round-bottom flask A 2.14 g sample of $S_2(CH_2CH_2CO_2H)_2$ (1.02 mmol) was added to the flask and allowed to dissolve followed by addition of 1.87 mmol (1.90 mL) of 4-(aminomethyl)pyridine dropwise over a period of 1 min with gentle stirring. A drying tube was attached to the 50 mL round-bottom flask, and the mixture was allowed to slowly stir at room temperature. After 24 h, the reaction mixture was removed and gravity filtered, to remove any large impurities, through a Whatman no. 1 filter paper into a clean 100 mL round bottom flask. With gentle heating, the THF was removed by rotary evaporation until dry. The light yellow-colored liquid that remained was further dried by vacuum, approximately 1 h, until no further bubbling of the liquid occurred. Then the product was twice purified from methanol and diethyl ether using the following procedure. First, the crude product was dissolved in a minimum amount of methanol. Next, the diethyl ether was slowly added dropwise to the mixture, resulting in a white precipitate at the drop/mixture interface, while swirling the flask so that no oiling occurred. Addition of diethyl ether continued until the solution just became cloudy. The mixture was then placed in a 5 °C freezer until fluffy white crystals developed, which were collected by suction filtration onto a medium-fritted glass filter. The product was washed with 5 × 10 mL of cold anhydrous ethyl ether, dried by suction, placed in a 100 mL round-bottom flask, and vacuum dried overnight. The yield was 942 mg (26%).

Characterization data for $\{(NC_5H_4)CH_2NHCO(CH_2)_2S-\}_2$ are as follows. ^{1}H NMR spectrum in CD_3Cl: δ 2.65 (2H, t), 3.05 (2H, t), 4.45 (2H, d), 6.60 (1H, s, br), 7.20 (2H, d), 8.55 (2H, d). Anal. Calcd. for $\{(NC_5H_4)CH_2NHCO(CH_2)_2S-\}_2$: C, 55.36; N, 14.35; H, 5.68. Found: C, 55.46; N, 14.22; H, 5.45. UV−visible [λ (nm), CH_3CN (ϵ in M^{-1} cm^{-1})]: 256 nm (4.44×10^3), 296 nm (5.70×10^2). FTIR−ATR (film dried on germanium plate) [ν(CO) cm^{-1}]: 1654.

fac-Re(bpy)(CO)$_3$(CF$_3$SO$_3$). The preparation of *fac*-Re(bpy)(CO)$_3$(CF_3SO_3) was accomplished by using previously published methods.[15]

{fac-Re(bpy)(CO)$_3$[(NC$_5$H$_4$)CH$_2$NHCO(CH$_2$)$_2$S−]$_2$} (CF$_3$SO$_3$). A 268 mg sample of $[(NC_5H_4)CH_2NHCO(CH_2)_2S-]_2$ (0.687 mmol) was dissolved in a minimum amount of anhydrous absolute ethanol in a 100 mL two-neck round-bottom flask. In a separation, 385 mg sample of *fac*-Re(bpy)(CO)$_3$(CF_3SO_3) (0.670 mmol) was added to 45 mL of anhydrous absolute ethanol. This mixture was heated slowly with stirring until the solid dissolved. The ethanol *fac*-Re(bpy)(CO)$_3$(CF_3SO_3) mixture was then transferred into a 125 mL addition funnel in one of the necks of the 100 mL reaction flask containing the ethanol−ligand mixture. A reflux condenser, with a drying tube open to the atmosphere, was placed in the other neck of the reaction flask and the reaction mixture brought to reflux temperature. At this time, the ethanol−*fac*-Re(bpy)(CO)$_3$(CF_3SO_3) mixture was added dropwise to the reaction mixture at a rate of 6 drops/min. After addition was complete, the total reaction mixture, now containing both the *fac*-Re(bpy)(CO)$_3$(CF_3SO_3) and $[(NC_5H_4)CH_2NHCO(CH_2)_2S-]_2$, was refluxed over a 48 h period. The entire procedure was performed in air. The reaction mixture was allowed to cool and then transferred to a single neck 250 mL round bottom flask. Upon removal of the solvent by rotary evaporation, the light yellow crude product began to crystallize. The product was placed under vacuum overnight and then diluted with fresh diethyl ether. A drying tube was placed on the flask and the solution stirred at room temperature. The diethyl ether was changed with fresh solvent after a few hours and the stirring process repeated. After repeated stirring, the product was isolated as a crystalline material on the sides of the flask. The yield was 605 mg (93%).

Characterization data for {*fac*-Re(bpy)(CO)$_3$[(NC$_5$H$_4$)CH$_2$NHCO(CH$_2$)$_2$S−]$_2$} (CF_3SO_3) are as follows. ^{1}H NMR spectrum in $CDCl_3$: δ 2.60 (6H, m, br), 2.90 (6H, m, br), 4.25 (2H, d), 4.40 (2H, t), 6.60 (2H, s, br), 7.20 (6H, m, br), 7.60 (2H, s, br), 7.80 (4H, m, br), 7.93 (2H, d), 7.97 (1H, d), 8.27 (2H, m, br), 8.40 (1H, s), 8.45 (2H, t), 8.55 (1H, d), 8.60 (1H, d), 9.15 (2H, t). Anal. Calcd. for {*fac*-Re(bpy)(CO)$_3$[(NC$_5$H$_4$)CH$_2$NHCO(CH$_2$)$_2$S−]$_2$} (CF_3SO_3): C, 39.06; N, 8.54; H, 3.28. Found: C, 39.10; N, 8.38; H, 3.33. The ^{1}H NMR spectrum of this sample revealed a small fraction of ether present. UV−visible [λ(nm), CH_3CN (ϵ in M^{-1} cm^{-1})]: 250 nm (1.86×10^4), 306 nm (1.08×10^4), 320 nm (1.12×10^4), 344 nm (3.22×10^3). FTIR−ATR (film dried on germanium plate) [υ (CO) cm^{-1}]: 1657, 1916, 2031.

{fac-Re(bpy)(CO)$_3$(NC$_5$H$_4$)CH$_2$NHCO(CH$_2$)$_2$S−}$_2$(CF$_3$SO$_3$)$_2$. A 300 mg sample of {*fac-Re*(bpy)(CO)$_3$[(NC$_5$H$_4$)CH$_2$NHCO(CH$_2$)$_2$S−]$_2$}(CF_3SO_3) (0.310 mmol) was dissolved in 10 mL of anhydrous absolute ethanol in a 10 mL round-bottom flask with gentle heating and stirring. In a separate flask, 178 mg of Re(bpy)(CO)$_3$(CF_3SO_3) (0.310 mmol) was dissolved in 40 mL of absolute anhydrous ethanol with gentle heating and stirring. The ethanol−*fac*-Re(bpy)(CO)$_3$(CF_3SO_3) solution was transferred to a 125 mL addition funnel and the funnel placed in one of the necks of the 100 mL flask containing the ethanol−Re(bpy)(CO)$_3$(CF_3SO_3) solution. A small reflux condenser

containing a drying tube open to the atmosphere was placed into the remaining neck of the reaction flask. At reflux temperature, the ethanol−{*fac*-Re(bpy)$(CO)_3[(NC_5H_4)CH_2$-$NHCO(CH_2)_2S-]_2\}(CF_3SO_3)$ was added to the reaction mixture dropwise at a rate of 6 drops/min. The mixture was then gently heated at reflux for 72 h allowed to cool, and then transferred to a clean 250 mL round-bottom flask. Ethanol was removed from the mixture by rotary evaporation. What remained was a heavy yellow liquid, with no visible evidence of crystallization, as was the case in the {*fac*-Re(bpy)$(CO)_3[(NC_5H_4)CH_2NHCO$-$(CH_2)_2S-]_2\}(CF_3SO_3)$ synthesis discussed earlier. The crude product was further dried under vacuum for 12 h. Purification of the crude product was accomplished by continually washing the heavy yellow liquid, coating the walls of the flask, with fresh diethyl ether while stirring by placing a drying tube on the flask opening, and stirring vigorously at room temperature. The diethyl ether was changed twice more for a total of three washings, decanting off the waste solvent and pouring fresh solvent into the flask. The first two washings were changed after 3 h intervals, with the final washing stirred overnight. After the first washing, the heavy yellow liquid began to solidify, falling off the walls of the flask. The solid product was collected by suction filtration onto a medium-fritted glass filter and further washed with 5 × 10 mL of cold anhydrous ethyl ether. Reprecipitation was used to further purify the product. A fritted glass filter containing the product was placed over a 100 mL round-bottom flask and the product washed and gently stirred with fresh anhydrous ethyl ether. Methylene chloride was then added dropwise into the fritted filter containing the product. As the product dissolved, it was carried through the filter and dropwise added into the stirred ether, reprecipitating into fluffy yellow crystals. The solid was again collected by suction filtration using a medium glass-fritted filter and washed with 5 × 10 mL of cold anhydrous ethyl ether. The yield was 400 mg (82%).

Characterization data for {*fac*-Re(bpy)$(CO)_3(NC_5H_4)CH_2$-$NHCO(CH_2)_2S-\}_2$ $(CF_3SO_3)_2$ are as follows. ^{1}H NMR spectrum in CD_3CN: δ 2.50 (2H, t), 2.85 (2H, t), 4.25 (2H, d), 7.05 (1H, s, br), 7.15 (2H, d), 8.12 (2H, d), 8.25 (2H, m), 8.35 (2H, d), 8.45 (1H, d), 9.00 (1H, d), 9.18 (2H, d). Anal. Calcd. for {*fac*-Re(bpy)$(CO)_3(NC_5H_4)CH_2NHCO(CH_2)_2S-\}_2(CF_3$-$SO_3)_2$: C, 33.94; N, 6.74; H, 2.65. Found: C, 34.37; N, 6.70; H, 2.67. The ^{1}H NMR spectrum of this sample revealed a small fraction of ether present in the sample. UV−visible [λ (nm), CH_3CN (ϵ in M^{-1} cm^{-1})]: 248 nm (2.49×10^4), 306 nm (1.64×10^4), 318 nm (1.72×10^4), 338 nm (5.00×10^3). FTIR−ATR (film dried on germanium plate) [υ(CO) cm^{-1}]: 1664, 1913, 2031.

Preparation of Self-Assembled Monolayers. *Surface Plasmon Spectroscopy and Ellipsometry*. After the initial plasmon spectrum of the pure Ag- or Au-coated substrate slides was obtained to determine the optical constants and thicknesses of these metal films, the index-matching fluid was removed from the back of the slide by thoroughly rinsing with absolute ethanol. The slide was then immediately immersed in a 1 mM solution of ligand **L1**, or the appropriate metal complex **C1** or **C2**, in absolute ethanol (see schemes 1 and 2 for structural formulas of these molecules). The monolayer was allowed to spontaneously self-assemble onto the thin metal films for 24 h. Longer time periods of 48 and 72 h were examined with no apparent experimental effect on monolayer formation and thickness. After the 24 h period, the slide was removed and rinsed with fresh absolute ethanol and dried with a light stream of dry N_2. It was found through previous experimentation that the use of separate slides for obtaining the ellipsometric and plasmon data made no difference over using one slide for both surface measurement methods. However, separate slides were used for both the surface plasmon and ellipsometric measurements to minimize contamination of the metal films by limiting exposure time to air.

SERS and FTIR Preparations. The silver foil substrates were immersed in a 1 mM solution of **L1**, **C1**, or **C2** in anhydrous absolute ethanol for 24 h. Prior to the SERS adsorption studies, the silver foil substrates were removed from the metal complex solutions, rinsed with absolute ethanol, and dried in a stream of N_2. Germanium plates were cleaned with ethanol for the solid-state reflectance FTIR measurements.

Measurements. *Surface Plasmon Spectroscopy*. The method used for surface plasmon detection was attenuated total reflectance (ATR) spectroscopy. All SPS data were collected using the short-range Krestchmann optical configuration as described previously.[14] The surface plasmon is generated by using a p-polarized 6328 Å line from a Spectra Physics Model 151-P 1 mW CW HeNe laser. The ATR reflectivity curve was obtained using a Ge photodiode/op-amp detector connected to a Data Translation DT2801A data acquisition board (DAB) interfaced to a 486 PC. The computer is also interfaced to a optically encoded, DC motor-driven rotation stage. A program written in ASYST records the digitized ATR curve in terms of reflectivity, ranging from 0 to 1, as a function of prism rotation angle. The reflectivity for each experimental run is corrected for background noise and normalized from a voltage to a reflectivity scale ranging from 0 to 1.

Surface plasmon apparatus, measurement, and theory as we use it in this work have been discussed elsewhere.[14,16,17] The ATR resonance curve due to plasmon generation is extremely sensitive to variations in the refractive index and thickness of the dielectric at the metal−dielectric interface. The unique shape and angular position of the minimum of the pure metal SPS resonance curve are determined by its thickness (*d*) and complex index (*n* and *k*). After self-assembly of the complexes to the Ag or Au metal film, the optical thickness and complex index or dielectric of the SAM film changes the refractivity of the combined films, thereby changing the shape and angular position of the ATR minimum. From this resonance curve shift and knowledge of the optical thickness and complex index of the metal, the thickness and refractive index of the SAM can be determined as explained previously using a nonlinear least-squares procedure.[14] At 6328 Å, the SAM films examined in this study present no absorption or imaginary index component. Therefore, a single wavelength SPS curve can uniquely determine the thickness and real index of the SAM from the reflectivity versus angular position of the SPS spectrum. However, the thickness and complex index of the pure metal film cannot be uniquely determined at a single wavelength. In our previous SPS work on Ag/Au bimetallic films at 6328 Å, this limitation has not precluded a determination of these three parameters that are consistent with known literature values.[18] Our experimental benefit rests in a very accurate and precise nonlinear fitting of the SPS curves in what we have called "exact" fits with extremely small residuals that were never greater than ±1% in the worst case. In fact, nonlinear least-squares fits of the combined metal/SAM film with known metal parameters and unknown SAM parameters (*d*, *n*, obtained *k*) results in a null contribution to the imaginary index. An estimate of the accuracy for plasmon-determined thicknesses found in Table 1 below, based on the residuals fit, is ±1 Å for both Ag and Au.

SERS and FTIR Spectroscopy. Surface-enhanced Raman spectra were obtained with a Spectra Physics 2025 water-cooled Kr^+ operating at 647.1 nm. The SERS signal was focused into

TABLE 1: Comparison of Plasmon and Ellipsometric Thicknesses for Ligand and Organometallic Complexes[a]

	gold			silver		
	plasmon[a]		ellipsometric	plasmon[a]		ellipsometric
monolayer[b]	index	thick	thickness	index	thick	thickness
L2	1.29	8	9	1.34	11	10
C3, **L2**	1.31	12	12	1.37	12	15
C3	1.31	12	16	1.34	15	16

[a] Plasmon index and thickness values are obtained from the curve fit. [b] Refer to Figure 1 for identification of the ligand and organometallic compounds. An estimate of the accuracy for the plasmon-determined thicknesses, based on the residuals fit, as ±1 Å for both silver gold. We estimate the accuracy at ±2 Å for the ellipsometric thicknesses. [c] Thickness values are in angstrom units.

a ISA HR-320 spectrograph connected to a Photometrics CCD9000 charged coupled device (CCD) detector, which was held at −102 °C. A 386 computer was used to collect, store, and plot the data. The reflectance (ATR) infrared spectra of both metal complexes and the ligand were collected using a Bomem MB 102 FTIR.

NMR Spectroscopy. ^{1}H NMR spectral data were collected using a JEOL 270 MHz NMR spectrometer. CD_3Cl was used as the solvent for the ligand, and CD_3CN was used for the organometallic complexes. Spectra were referenced to excess protio peaks in the solvent.

UV and Visible Spectroscopy. Ultraviolet and visible spectra were obtained using a Hewlett-Packard 8452A diode array spectrophotometer. Samples were placed in a 1.00 cm quartz cuvette and were referenced to a solvent blank. Extinction coefficients were obtained from samples with absorbances between 0.1 and 1.

Ellipsometric Film Thickness. A Rudolph Research Auto EL^R-II instrument was used at 632.8 nm to obtain the ellipsometric data at a constant reflectance angle of 140° by averaging measurements recorded from four separate spots on each slide. A computer program, written by Rudolph Research, was used to determine the index and monolayer thickness. In our protocol, the film thickness of the bare metal film was obtained first with SPS followed by ellipsometric and SPS measurements of the combined metal−SAM films. We emphasize that the refractive indices used in calculation of the ellipsometric monolayer thicknesses were from the surface plasmon measurements. Ellipsometric results reported in Table 1 are averages recorded from four separate spots on each slide.

Contact Angle Measurements. A Ramé-Hart Model 100−00 115 goniometer was used for the contact angle measurements using Millipore water in air as the probe liquid. Both advancing (θ_a) and equilibrium (θ_e) contact angle measurements were recorded. The advancing measurement were taken according to the protocol discussed by Walczak,[19] while the equilibrium contact angle was obtained after allowing sufficient time for the water droplet to come into equilibrium with the slide surface. In this study, contact angles are used as a qualitative measurement for comparison to previous values[19,20] where monolayers were self-assembled from absolute ethanol.

Results and Discussion

Preparation of Organometallic Compounds. In order to anchor the Re−carbonyl complexes to a Ag or Au surface, it was necessary to prepare a ligand that was capable of binding strongly to both the Re center and the surface of interest. Following literature precedents,[15] a pyridine donor containing a disulfide was chosen as the synthetic target. As shown in Scheme 1 the new ligand **L1** was synthesized by reacting

SCHEME 1

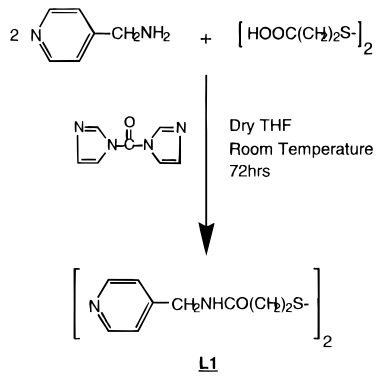

SCHEME 2

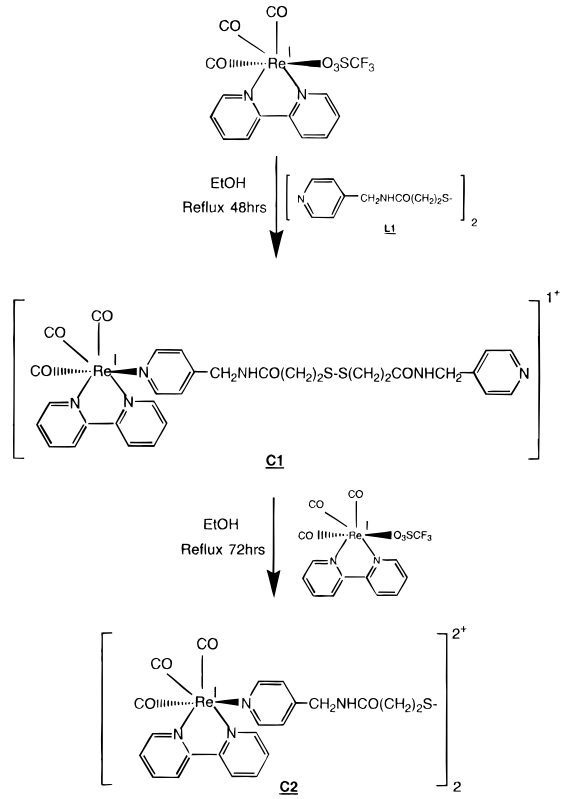

dithiodipropionic acid in slight excess with 4-(aminomethyl)-pyridine in the presence of the coupling agent carboxyldiimidizole in THF. After recrystallization, **L1** was obtained as fluffy white crystals in 26% yield and was subsequently in the metal complex preparation.

Scheme 2 shows the preparation of the metal complexes **C1** and **C2** as their triflato salts by reaction with the reactive precursor *fac*-Re(CO)$_3$(bpy)(CF$_3$SO$_3$). This latter complex has been demonstrated to be extremely useful in the preparation of a wide variety of *fac*-Re(CO)$_3$(chelate)L^{n+} complexes.[15] Complex **C1** was first synthesized by reacting equimolar equivalents of **L1** and *fac*-Re(CO)$_3$(bpy)(CF$_3$SO$_3$) in ethanol. After purification (see Materials section) the light-yellow complex was obtained in high yield (93%). Reaction of **C1** with an equimolar amount of *fac*-Re(CO)$_3$(bpy)(CF$_3$SO$_3$), again in anhydrous ethanol, gave an 82% yield of fluffy yellow crystals of **C2**. Both complexes and the new ligand were characterized by UV−visible, NMR, and infrared spectroscopies, in addition to chemical analysis.

In the molecular mechanics analysis (discussed below) and the projection analysis, tilt angles increase or remain the same,

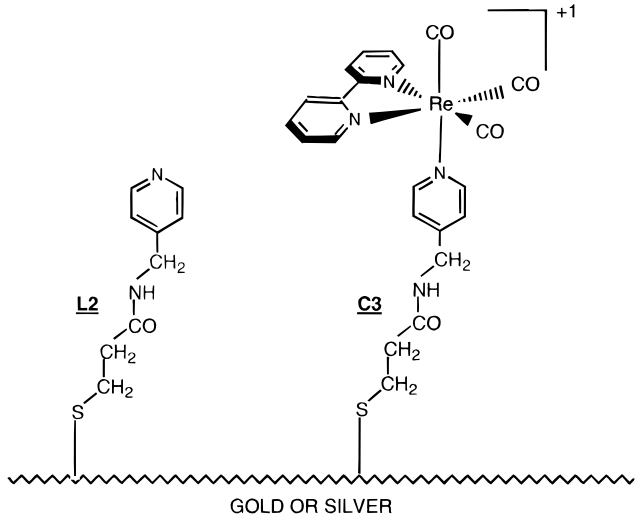

Figure 1. Schematic diagram representing the SAM of an **L1**, **C1**, and **C2** molecule attached to the Ag or Au surface. **L1** is bonded as an **L2** SAM, the **C1** complex is bonded as **L2**−**C3** SAM, and the **C2** complex is bonded as a **C3** SAM.

TABLE 2: Tilt Angles[a] for Ligand and Organometallic Complexes

	tilt angle			
	Au		Ag	
monolayer[b]	projection	molecular mechanics	projection	molecular mechanics
L2	35	33	24	19
C3-L2	23	32	28	31
C3	34	41	25	34

[a] The reported molecular tilt angles are referenced to the metal surface normal. [b] Refer to Figure 1 for identification of the ligand and organometallic compounds. We estimate the error in tilt angle determined by projection analysis to be ±2°. Those determined by molecular mechanics are in need of further refinement (see text).

respectively, as the monolayer changes from pure ligand **L2** to pure complex **C3** with the exception of the mixed **C3**−**L2** SAM case, which does not follow this trend (Figure 1). The metal complex **C1**, when attaching to the Au or Ag surface, will react at the disulfide bond, giving one molecule of **L2** and one molecule of **C3**. Our Raman results, discussed below, verify this conclusion. But when thermal equilibrium is reached between the metal surface and the solution of the **C1** disulfide, the precise molecular surface morphology, **L2**−**L2**−**L2**−**C3**−**L2**−**L2**−, cannot be predicted from our study. As the **C1** molecules bond to the metal surface, they will ultimately assemble in the most stable configuration. And this assembly may take the form of two or more organic ligands **L2** for every bulk organometallic molecule **C3**. This molecular configuration could reasonably account for the irregularity of the tilt angles of the this SAM found in Table 2. Note that the morphology of bonding of the partners of an alkane−disulfide molecule to a Au surface varies depending on interpretation.[23]

Grouped pairs of ATR resonance curves, reflectivity versus internal angle at the base of the prism, as shown in Figure 2. The narrower, left, pair is for Ag and the broader, right, pair corresponds to Au. Note that the characteristic position and shape of the plasmon spectrum is dictated by the pure metal film, left partner of the pair located at the lower internal angle. The right partner of the pair is the disulfide complex **C2** bonded to the metal in terms of a **C3** sulfide unit SAM as illustrated in Figure 1. These metal−SAM curves are shifted slightly, ~0.12°, toward higher angles because of the increased thickness of the SAM. We have not included the experimental curves

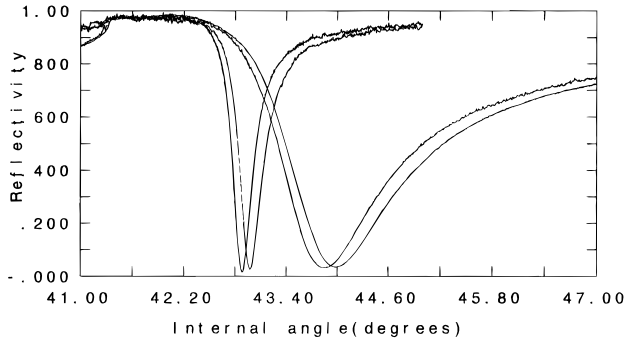

Figure 2. Experimental surface plasmon resonance curves of pure Ag and Au with attached **C3** SAMs. The narrower, left, pair is for Ag and the broader, right, pair corresponds to Au. The pure metal film, left partner of the pair, is located at the lower internal angle. The right partner of the pair is that of the disulfide complex **C2** bonded to the metal in terms of a **C3** sulfide unit SAM as illustrated in Figure 1.

for **L1** bonded as an **L2** SAM or the **C2** complex bonded as **L2**−**C3** SAM, also shown in Figure 1, since they are very similar in shape and angular position to the **C3** SAM shown. Table 1, below, summarizes the results for both the plasmon and ellipsometric thickness values of the ligand and metal complexes assembled on Ag and Au. Plasmon thickness reported were obtained by averaging data from four sets of slides, recording one spot per slide. Randomly selecting other spots on a single slide made no difference in the thickness analysis. We estimate the plasmon thickness accuracy at ±1 Å for both Ag and Au. Plasmon-determined refractive indices listed in Table 1 for the organic and organometallic SAMs were used in calculating the corresponding ellipsometric thickness. This method was also used in calculating the ellipsometric thicknesses in our recent plasmon study of alkanethiols,[21] since it is not possible to independently determine both the thickness and the real component of the index with an ellipsometric measurement at constant arm angle and wavelength. We estimate the ellipsometric thickness accuracy at ±2 Å for either Ag and Au, based on our experimental sampling that averaged four readings for four separate spots on a single slide. We do not understand the basic source of the increased uncertainty in the ellipsometric thicknesses, since this discrepancy was not found in our alkanethiol study. Within Table 1, the trend for ligand and metal complex molecules attached to Ag and Au shows that the ellipsometric and plasmon thickness measurements are generally larger for an identical molecule bonded to Ag than to Au. This trend agrees with previous relative thickness values obtained from a plasmon−ellipsometric study of different length alkanethiols[21] $HS(CH_2)_nCH_3$ (n = 11, 13, 15, 17, 19) bonded to Au and Ag. The previous alkanethiol study,[21] where there was a large variation in the methylene chain length, clearly showed an increase in the refractive index of the SAM with increasing SAM thickness. This trend was not unexpected and was attributed to differences in packing and consequent bulk polarizability $\chi^{(1)}$ changes affected by the alkyl chain length. Because of the narrow range in thicknesses seen in this study of rhenium complexes, we cannot state with certainty that the variation in the reported indices in Table 1 is correlated to SAM thicknesses and corresponding packing differences, but we believe this to be the case.

Table 2 summarizes the tilt angles of the ligand **L2**, the ligand−metal complex **L2**−**C3**, and the metal complex **C3** with respect to the metal surface normal. Tilt angles for the identical SAM on Ag are less than those on Au except for the mixed **L2**−**C3** SAM, which is intermediate. We have shown,[21] in agreement with Porter[19,22] and co-workers, that alkanethiols assembled on Au have a larger tilt angle than do the same thiols

TABLE 3: Contact Angle Measurements[a] for Ligand and Organometallic Complexes

	gold		silver	
monolayer[b]	advancing	equilibrium	advancing	equilibrium
water	94	90	90	88
L2	47	40	61	46
C3−**L2**	59	53	68	56
C3	69	63	69	59

[a] All contact angle measurements are in degrees. [b] Refer to Figure 1 for identification of the ligand and organometallic compounds.

on Ag. This trend is also evident in our tilt angle analysis in this study. Tilt angles reported in Table 2 were calculated in one of two ways, a *projection* analysis or a *molecular mechanics* calculation, each referenced to the surface normal of the metal. In the projection analysis we estimate the error in tilt angle to be ±2°. Projection tilt angles were determined using the longest length, S atom to axial CO in the metal complex **C3** or S atom to the N atom found in the pyridine group of the **L2** ligand, of the free, gas phase molecule and the experimentally determined plasmon SAM thicknesses. S-metal distances, 1.9 Å Au and 2.3 Å for Ag, were obtained from work by Sellers[23] and co-workers. The molecular length was calculated using the minimization procedure and MMX force field, including paramatrization for an octahedral Re, found in the molecular modeling software PCMODEL (V5.13, Serena Software, Bloomington, IN). The MMX force field used in PCMODEL is derived from the MM2 (QCPE-395, 1977) force field of N. L. Allinger,[24] with the π-VESCF routines taken from MMP1 (QCPE-318), also by N. L. Allinger.[25] MMX increased the number of atom types for the MM2 force field and added the ability to handle transition metals and transition states.

The second method of estimating the tilt angles, tabulated under the molecular mechanics columns in Table 2, involved the geometric optimization of the ligand **L2** or complex **C3** bonded to Au(111) and Ag(111) surfaces minimized using the PCMODEL program. The force constant parameters utilized for sp hybridized sulfur in our tilt angle calculations were obtained from previous work by Sellers[23] and co-workers. Sellers in fact calculated tilt angles for both sp^3 and sp hybridized sulfur attached to Au but only sp for Ag. His results indicated, modeling only a 16-carbon length alkanethiol, no relative difference in the absolute tilt, ~30°, for either sp^3 or sp hybridized sulfur on Au. We have therefore modeled **C3** and **L2** on both Ag and Au using only sp hybridized sulfur. For the calculation, **C3** and **L2** units were attached to a hollow metal site following a hexagonal surface coverage geometry, six units surrounding one, specified in Scheme 1 of ref 23. In the case of the mixed **C3**−**L2** SAM, the hexagonal arrangement of the **C3** and **L2** units alternated with **L2** in the center. The average molecular tilt angles were calculated from the surface of the metal to the terminal atom. Results reported in Table 2 are without benefit of a global energy minimum search. As such, they should be regarded as very crude, but the similarity to the tilt angles determined by the projection method suggests that our analysis is sensible.

In Table 3, the order of hydrophobicity is seen to be **C3** > **C3**−**L2** > **L2**. This trend cannot be easily understood, since it is a convoluted function of head-group polarity (functional group, size, metal complex charge, and triflate counterion) and packing density. Our results indicate that surface packing density dominates over polarity. In agreement with our **C3** measurement, Sullivan and co-workers[26] found that a monolayer with surface functionality −(Si)−$(CH_2)_4$(Mebpy)-*fac*-Re$(CO)_3$-Cl, where −(Si)− denotes surface siloxane bonding, exhibited an advancing contact angle of 69°. That work,[26] with similar

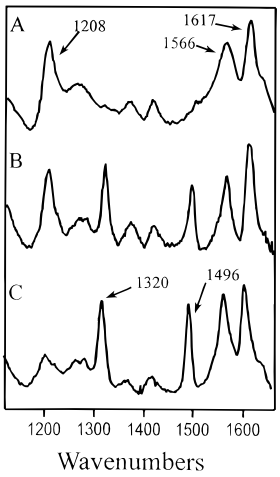

Figure 3. SERS spectra of the thiolate monolayers on Ag: (A) SERS spectrum of **L2**: (B) SERS spectrum of **L2**−**C3**; (C) SERS spectrum of **C3**.

ligands, also suggests that surface coverage for **L2** should be greater, perhaps as much as 10 times more than that for **C3**. **C3**−**L2** is expected to be intermediate in surface coverage.

SERS and FTIR Results. Representative SERS spectra of **L2**, **L2**−**C3**, and **C3** are shown in Figure 3. The **L2** spectrum, Figure 3A, is dominated by the quadrant ring modes of pyridine at 1566 and 1612 cm^{-1} and the in-plane C−H deformation at 1208 cm^{-1}.[27] Parts B and C of Figure 3 show the spectra of **L2**−**C3** and **C3**, respectively. It is clear from these spectra that the *fac*-Re(bpy)$(CO)_3$ has remained attached to **L2** during the formation of the SAM on the silver surface. The most significant difference between the SERS spectrum of **L2** and the spectra of **L2**−**C3** and **C3** is the appearance of two bands at 1320 and 1496 cm^{-1}. These correspond to the bridging C−C bond between the pyridine rings and a ring stretch, respectively. A comparison of the intensities in parts A−C of Figure 3 shows an interesting trend. The intensity of the pyridine ring modes in *fac*-Re(bpy)$(CO)_3$ is relatively stronger in comparison with these ligand Raman features in **C3** than for **L2**−**C3**. This is consistent with the presence of more (about twice as much) *fac*-Re(bpy)$(CO)_3$ per thiol self-assembled on the surface. However, measurement of the relative intensity of the **L2** mode at 1208 cm^{-1} and the intensity of the bipyridine bridge mode of the rhenium complex at 1320 cm^{-1} shows this intensity ratio to be 1:3, respectively. It is well-known that the intensity of SERS drops off exponentially as the scatterer moves further from the SERS substrate and that there is a strong orientational dependence as well. If the *fac*-Re(bpy)$(CO)_3$ group is free to rotate, this increase in intensity cannot be attributed to an orientational effect. On the other hand, if the self-assembly process induces a preferred orientation when the monolayer is composed of pure **C3** rather than the mixture **L2**−**C3**, then it is conceivable to see a 3-fold increase in the intensity of the *fac*-Re(bpy)$(CO)_3$ bipyridine modes in comparison to the **L2** pyridine deformation mode. Comparative SERS data for **L2**, **L2**−**C3**, and **C3** indicates that self-assembly of the **C3** complex, *fac*-Re(bpy)-$(CO)_3$−**L1**, has occurred.

In order to further characterize the **L1**, **C1**, and **C2** molecules, we have obtained FTIR−ATR spectra on thin films of these compounds dried on germanium plates. It is important to recognize that even though the microsymmetry of the rhenium complex *fac*-Re(2,2′-bipyridine)$(CO)_3$pyridine^{+1} found in complexes **C1**, **C2**, and **C3** is C_s, the effective geometrical symmetry is in fact C_{3v} because of the electronic similarity of the bipyridine and pyridine ligands surrounding the rhenium. The free rhenium cation complexes **C1** and **C2** each show one poorly resolved,

broad band at 1916 and 1913 cm^{-1}, respectively, and one sharp band located at 2031 cm^{-1} for both compounds. These modes are assigned to the carbonyls bound to the rhenium. As previously[28−30] reported, the IR spectrum of C_s rhenium complexes, having relatively the same structure as ours with the exception of the pyridine being replaced by a chloride, exhibited two a′ symmetrical modes and one a″ asymmetrical mode. Through labeling experiments,[28] it was reported that the highest energy a_1' mode had a larger contribution from the two CO groups *cis* to the chloride ligand than did the lower energy a_2' mode, which had a larger contribution from the single CO group *trans* to the chloride. Assuming C_{3v} symmetry in our case, we expect to see only two IR active carbonyl modes, a_1 and e detailed above, since the e mode correlates with the a″ and a_2' modes in C_s symmetry. Based on a comparison of *fac*-Re(2,2′-bipyridine)$(CO)_3$pyridine^{+1} spectrum to the published *fac*-Re(2,2′-bipyridine$(CO)_3$Cl spectrum, we conclude this doublet is due to an incomplete $C_s \rightarrow C_{3v}$ transition. We have assigned the bands found at 1654, 1657, and 1664 cm^{-1} for **L1**, **C1**, and **C2**, respectively, to the carbonyl mode for the amide that is found in the aliphatic chain by comparing the IR spectrum of **L1** to the spectra of **C1** and **C2**. The stretching frequencies of the rhenium carbonyls cation complexes are higher than those of *fac*-Re(2,2′-bipyridine)$(CO)_3$Cl complex, which we attribute to the decrease in π-backbonding between the rhenium and the carbonyl groups when the chloride is replaced with a pyridine.[28,30,31] The SERS data of the SAMS **L2**, **L2**−**C3**, and **C3** on Ag are in good agreement with the FTIR results discussed above.

Conclusions

We have shown that bulk surface plasmon spectroscopy can be used to characterize the attachment of rhenium disulfide complexes to Ag or Au on a molecular level. This method allows for not only the index of refraction and thickness of the film to be measured but also the relative bulk molecular orientation of attachment to the metal surface. SERS and FTIR data have also been used to corroborate the conclusion that our synthesized molecules self-assemble on Ag and Au. Comparative SERS data for **L2**, **L2**−**C3**, and **C3** indicate that self-assembly of the **C3** complex, *fac*-Re(bpy)$(CO)_3$−**L1**, occurred via thiol linkage to the silver surface.

From a preparative point of view, the Re complexes have several desirable features including the ability to easily vary the type of polypyridine ligand. Utilizing these properties, we are now in a position to begin sequential monolayer deposition. Besides having the potential for exhibiting large nonlinear properties, rhenium tricarbonyl complexes of this type are relatively easy to synthesize compared to other organometallics, exhibit very good stability in air, and allow for ready derivitization at the non-carbonyl sites.

Acknowledgment. We thank Professor Dan Buttry for use of his Edwards evaporator, ellipsometer, and goniometer. We also express our thanks to the Research Corporation for support of this research. N.M. gratefully acknowledges support of his 1995 Summer Arts and Sciences College Independent Study fellowship.

References and Notes

(1) *Nonlinear Optical and Electroactive Polymers*; Prasad, P. N., Ulrich, D. R., Eds.; Plenum: New York, 1987.
(2) Ulman, A. *An Introduction to Ultrathin Organic Films*; Academic: New York, 1991.
(3) Roberts, G. G. In *Electronic and Phonic Applications of Polymers*; Bowden, M. J., Turner, S. R., Eds.; Advances in Chemistry Series 218; American Chemical Society: Washington, DC, 1988; p 225.
(4) Prasad, P. N.; Williams, D. J. *Nonlinear Optical Effects in Molecules and Polymers*; John Wiley and Sons, Inc.: New York, 1991.
(5) Girling, I. R.; Cade, N. A.; Kolinsky, R. J. J.; Peterson, I. R.; Ahmad, M. M.; Neal, D. B.; Petty, M. C.; Roberts, G. G.; Feast, W. J. *J. Opt. Soc. Am. B* **1987**, *4*, 950.
(6) Corn, Robert M.; Hanken, Dennis G. *Anal. Chem.* **1995**, *67*, 3767.
(7) Ulman, A.; Evans, S. D. *J. Am. Chem. Soc.* **1991**, *113*, 5866.
(8) Lee, H.; Mallouk, T. E.; Kepley, L. J.; Hong, H.-G.; Akhter, S. *J. Phys. Chem.* **1988**, *92*, 2597.
(9) Lee, H.; Hong, H.-G.; Mallouk, T. E.; Kepley, L. J. *J. Am. Chem. Soc.* **1988**, *110*, 618.
(10) Wrighton, M. S.; Morse, D. L. *J. Am. Chem. Soc.* **1974**, *96*, 998.
(11) Sullivan, B. P.; Bolinger, C. M.; Conrad, D.; Vining, W. J.; Meyer, T. J. *J. Chem. Soc., Chem. Commun.* **1985**, 1414.
(12) Calabrese, J. C.; Tam, W. *Chem. Phys. Lett.* **1987**, *133*, 244.
(13) Sullivan, B. P. *J. Phys. Chem.* **1989**, *93*, 24.
(14) Ehler, T. T.; Noe, L. J. *Langmuir* **1995**, *11*, 4177.
(15) Sullivan, B. P.; Hino, J. K.; Ciana, L. D.; Dressick, W. J. *Inorg. Chem.* **1992**, *31*, 1072.
(16) Sprokel, G. J.; Santo, R.; Swalen, J. D. *J. Mol. Cryst. Liq. Cryst.* **1981**, *68*, 29.
(17) Sprokel, G. J. *J. Mol. Cryst. Liq. Cryst.* **1981**, *68*, 39.
(18) Johnson, P. B.; Christy, R. W. *Phys. Rev. B* **1972**, *6*, 4370.
(19) Walczak, M. M.; Chung, C.; Stole, S. M.; Widrig, C. A.; Porter, M. *J. Am. Chem. Soc.* **1991**, *113*, 2370.
(20) Laibinis, P. E.; Whitesides, G. M.; Allara, D. L.; Tao, Y.-T.; Parikh, A. N.; Nuzzo, R. J. *J. Am. Chem. Soc.* **1991**, *113*, 7152.
(21) Ehler, T. T.; Malmberg, N.; Noe, L. J. *J. Phys. Chem. B*, in press.
(22) Porter, M. D.; Bright, T. B.; Allara, D. L.; Chidsey, C. E. D. *J. Am. Chem. Soc.* **1987**, *109*, 3559.
(23) Sellers, H.; Ulman, A.; Shnidman, Y.; Eilers, J. E. *J. Am. Chem. Soc.* **1993**, *115*, 9398.
(24) Allinger, N. L. *J. Am. Chem. Soc.* **1977**, *99* (25), 8127.
(25) Allinger, N. L. *Adv. Phys. Org. Chem.* **1976**, *13*, 1.
(26) Sullivan, B. P.; Morris, K.; Paulson, S. *J. Chem. Soc., Chem. Commun.* **1992**, 1615.
(27) Daimay, L.-V.; Colthup, N. B.; Fateley, W. G.; Grasselli, J. G. *The Handbook of Infrared and Raman Characteristic Frequencies of Organic Molecules*; Academic Press, Inc.: San Diego, CA, 1991.
(28) George, M. W.; Johnson, F. P. A.; Westwell, J. R.; Hodges, P. M.; Turner, J. J. *J. Chem. Soc., Dalton Trans.* **1993**, 2977.
(29) Houk, L. W.; Dobson, G. R. *J. Inorg. Chem.* **1966**, *5*, 2119.
(30) Edwards, D. A.; Marshalsea, J. *J. Organomet. Chem.* **1977**, *131*, 73.
(31) Staal, L. H.; Oskan, A.; Vrieze, K. *J. Organomet. Chem.* **1979**, *170*, 235.